Chirp-Scaling based True Amplitude Imaging for Synthetic Aperture Radar

Ling Wang[a,b], Can Evren Yarman[c] and Birsen Yazıcı[a]

[a]Electrical, Computer, and System Engineering Department, Rensselaer Polytechnic Institute, Troy, NY 12180 USA;
[b]Information and Communication Engineering, Nanjing Unversity of Aeronautics and Astronautics, Nanjing, Jiangsu 210016 China;
[c]Houston Technology Center, WesternGeco-Schlum-berger, Houston, TX 77042 USA

ABSTRACT

The Chirp-Scaling Algorithm (CSA) is one of the most widely used synthetic aperture radar (SAR) image reconstruction method. However, its applicability is limited to straight flight trajectories and monostatic SAR. We present a new mathematical treatment of the CSA from the perspective of Fourier Integral Operators theory. Our treatment leads to a chirp-scaling-based true amplitude imaging algorithm, which places the visible edges of the scene at the correct locations and directions with the correct strength. Furthermore, it provides a framework for the extension of the chirp-scaling based approach to non-ideal imaging scenarios as well as other SAR imaging modalities such as bistatic-SAR[1] and hitchhiker-SAR.[2]

Keywords: Synthetic aperture radar (SAR), Imaging, Chirp-scaling algorithm (CSA), Filtered-backprojection (FBP), Fourier integral operator (FIO)

1. INTRODUCTION

The Chirp-Scaling Algorithm (CSA) is one of the most widely used synthetic aperture radar (SAR) image reconstruction method. It has the benefit of eliminating the interpolation for the range cell migration correction. However, CSA's applicability is limited to straight flight trajectories and monostatic SAR.

In Ref. 1 and 3, generalized filtered-backprojection (FBP) methods for monostatic and bistatic SAR have been developed for arbitrary flight trajectories using the theory of Fourier Integral Operators (FIO)s. The theory shows that the backprojection operator places the visible edges at the right locations and directions, but not with the correct strength. However, when combined with the filtering, backprojection based imaging methods place the visible edges at the right location, direction and right strength resulting in *true amplitude* imaging.

In this paper, we present a new mathematical treatment of the CSA from the perspective of FIO theory. Our treatment (i) leads to a chirp-scaling-based true amplitude imaging algorithm, (ii) provides a framework for the extension of the chirp-scaling based approach to non-ideal imaging scenarios as well as other SAR imaging modalities such as bistatic-SAR[1] and hitchhiker-SAR.[4]

Our paper is organized as follows: In Section 2, we state the SAR measurement model based on the scalar wave equation and the single-scattering assumption. In Section 3, we present the measurement model for CSA . In Section 4, we derive the CS inversion using the FIO theory and show that a true-amplitude image reconstruction based on the chirp-scaling can be achieved by appropriate selection of the filter in the FBP method suggested by the FIO approach. Finally, we conclude our discussion in Section 5.

Further author information: (Send correspondence to B.Y.)
B.Y.: E-mail: yazici@ecse.rpi.edu, Telephone:+1 (518) 276 2905, Fax: +1 (518) 276 6261
C.E.Y.: E-mail: yarman@ecse.rpi.edu
L.W.: wangl9@rpi.edu or wanglrpi@gmail.com

Algorithms for Synthetic Aperture Radar Imagery XVI, edited by Edmund G. Zelnio, Frederick D. Garber,
Proc. of SPIE Vol. 7337, 733707 · © 2009 SPIE · CCC code: 0277-786X/09/$18 · doi: 10.1117/12.819123

2. MEASUREMENT MODEL FOR SAR

Unless otherwise stated, the bold Roman, bold italic, and italic small letters will denote points in $\mathbb{R}^3$, $\mathbb{R}^2$, $\mathbb{R}$, repectively, i.e., $\mathbf{x} = (\boldsymbol{x}, x_3) \in \mathbb{R}^3$, with $\boldsymbol{x} \in \mathbb{R}^2$, and $x_3 \in \mathbb{R}$.

Let $\boldsymbol{\gamma}(s) \in \mathbb{R}^3$, $s \in \mathbb{R}$, be the trajectory of an airborne antenna and $\psi : \mathbb{R}^2 \to \mathbb{R}$, be a known smooth function representing ground topography. We present the earth's surface by $\mathbf{x} = (\boldsymbol{x}, \psi(\boldsymbol{x}))$ and assume that the scattering takes place in a thin region near the surface. Following 5,6, under the single-scattering (Born) approximation,[7,8] the ideal SAR received signal without noise and clutter can be modeled as:

$$d(s,t) \approx \mathcal{F}[T](s,t) := \int \mathrm{e}^{-\mathrm{i}2\pi f(t-2|\mathbf{r}_{s,\boldsymbol{x}}|/c_0)}\, A(\boldsymbol{x},s,f)\, T(\boldsymbol{x})\, df\, d\boldsymbol{x}, \tag{1}$$

where s denotes the slow-time (also referred to as azimuth-time) and t denotes the fast-time (also referred to as range-time); $\mathbf{r}_{s,\boldsymbol{x}} = \boldsymbol{\gamma}(s) - \mathbf{x}$ and $|\mathbf{r}_{s,\boldsymbol{x}}|$ is the distance between the radar at position $\boldsymbol{\gamma}(s)$ and the scattering point, $\mathbf{x}$; $T(\boldsymbol{x})$ denotes the ground reflectivity, c_0 denotes the speed of light in dry air and f is the temporal frequency. A is a complex amplitude function which includes the antenna beam pattern, the Fourier transform of the transmitted waveform and the geometrical spreading factor, $|\mathbf{r}_{s,\boldsymbol{x}}|^{-2}$.

We assume that for some m_A, A satisfies the symbol estimate[5,6]

$$\sup_{(s,\boldsymbol{x})\in\mathcal{C}_{s,\boldsymbol{x}}} \mid \partial_f^\alpha \partial_s^\beta \partial_{x_1}^{\rho_1} \partial_{x_2}^{\rho_2} A(\boldsymbol{x},s,f) \mid \leq C_0\ (1+f^2)^{(m_A-|\alpha|)/2} \tag{2}$$

where $\mathcal{C}_{s,\boldsymbol{x}}$ is any compact subset of $\mathbb{R}\times\mathbb{R}^2$, and the constant C_0 depends on $\mathcal{C}_{s,\boldsymbol{x}}, \alpha, \beta, \rho_1$, and ρ_2. This assumption is needed to be able to perform various stationary phase calculations. This assumption is valid, for example, when the antenna is broadband and the source waveform is a band-limited waveform. We note that A can be complex; it can thus be used to model non-ideal antenna behavior such as phase aberrations and frequency-dependent changes in the beam pattern.

Under assumption (2), $\mathcal{F}$ defines a *Fourier Integral Operator*[9–11] whose leading order contribution comes from those points lying in the critical set of the phase, i.e., the intersection of the illuminated surface and the sphere $\mathcal{E}(s) = \{\mathbf{x} : |\mathbf{r}_{s,\boldsymbol{x}}| = c_0 t/2\}$. Since $\mathcal{F}$ is a Fourier integral operator, an approximate inverse of $\mathcal{F}$ can be computed by a suitable back-projection operator.

The ideal image formation problem is to estimate T from knowledge of $d(s,t)$ for some range of s and t.

We rewrite (1) as

$$d(s,t) \approx \int a(\boldsymbol{x},s,t-2|\mathbf{r}_{s,\boldsymbol{x}}|/c)\, T(\boldsymbol{x})\, d\boldsymbol{x} \tag{3}$$

where $a(\boldsymbol{x},s,t)$ is the inverse Fourier transform of $A(\boldsymbol{x},s,f)$ defined by

$$a(\boldsymbol{x},s,t) = \int \mathrm{e}^{-\mathrm{i}2\pi f t}\, A(\boldsymbol{x},s,f)\, df. \tag{4}$$

The data model used in conventional SAR imaging can be viewed as a special case of (3) where it is assumed that the flight trajectory is linear, i.e., $\boldsymbol{\gamma}(s) = \mathbf{v}(s) + \mathbf{h}$ for some fixed velocity $\mathbf{v} = (\boldsymbol{v}, 0) \in \mathbb{R}^3$ and altitude $\mathbf{h} = (0,0,h) \in \mathbb{R}^3$, $h \geq 0$, over a flat topography, i.e., $\psi(\boldsymbol{x}) = 0$.[12] Furthermore, it is assumed that $a(\boldsymbol{x},s,t)$ has the following structure:[12]

$$a(\boldsymbol{x},s,t) = p(t)\, w_a(s). \tag{5}$$

Here, p denotes the transmitted pulse, which is assumed to be a narrow-band linear frequency-modulated (FM) signal:

$$p(t) = w_r(t)\mathrm{e}^{\mathrm{i}2\pi\left(f_0 t + \frac{K}{2}t^2\right)}, \tag{6}$$

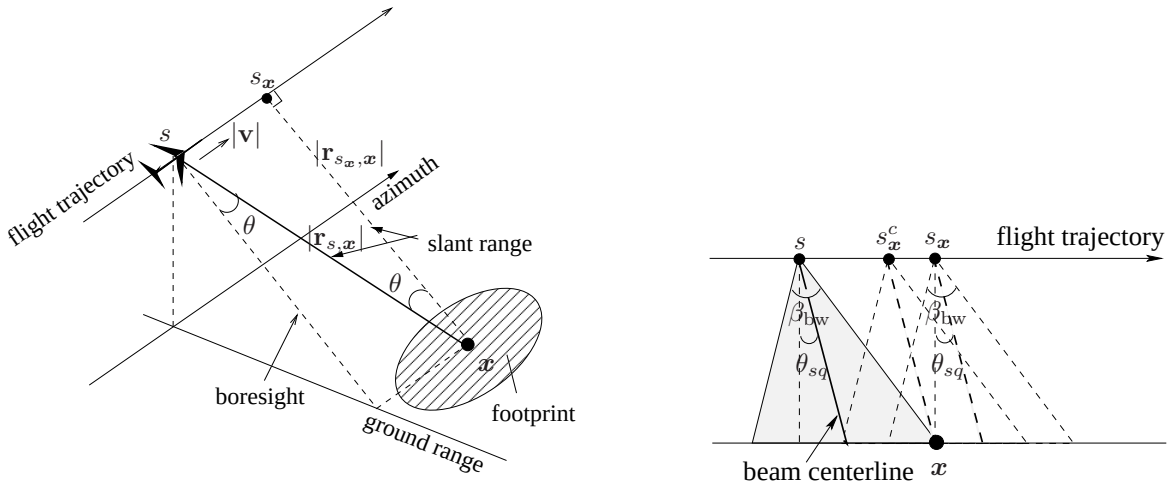

(a) (b)

Figure 1. SAR data collection geometry along with the definitions of SAR terminology: a) 3-D data collection geometry with the radar carrier at $\boldsymbol{\gamma}(s)$; b) 2-D data collection geometry on the slant range plane along with the azimuth antenna beam pattern.

where w_r is the envelope of p, typically assumed to be $\mathrm{rect}\,(t/\,T_0)$; T_0 is the pulse duration, f_0 is the center frequency and K is the FM rate. In (5), w_a is an amplitude modulation function due to the azimuth antenna beam pattern and is approximately given by

$$\mathrm{sinc}^2[0.886(\theta-\theta_{sq})/\beta_{\rm bw}] \tag{7}$$

where θ denotes the angle measured from the boresight to the vector, $\mathbf{r}_{s,\boldsymbol{x}}$, θ_{sq} denotes the squint angle of the antenna beam measured from the boresight to the beam center, and $\beta_{\rm bw} = c_0\,(f_0\,L_a)^{-1}$ is referred to as the azimuth beamwidth with L_a representing the antenna length in the azimuth direction.

Expressing the antenna beam pattern in terms of the slow-time, w_a in (5) is given by

$$w_a(s) \approx \mathrm{sinc}^2\left[0.886\,\arctan\left(|\mathbf{v}|\,(s-s^c_{\boldsymbol{x}})/|\mathbf{r}_{s_{\boldsymbol{x}},\boldsymbol{x}}|\right)/\beta_{\rm bw}\right] \tag{8}$$

where $s^c_{\boldsymbol{x}}$ denotes the slow-time when the beam center illuminates $\boldsymbol{x}$, $|\mathbf{r}_{s_{\boldsymbol{x}},\boldsymbol{x}}|$ denotes the "range of closest approach", i.e., the slant range when the radar is closest to $\boldsymbol{x}$ and $s_{\boldsymbol{x}}$ denotes the slow-time when $\boldsymbol{x}$ has zero-Doppler. Fig. 1(a) and 1(b) illustrate the SAR concepts described above.

From (3), (6) and (8), the base-band SAR data for linear flight trajectory can be expressed as follows:

$$d_0(s,t) = d(s,t)\,\mathrm{e}^{-\mathrm{i}2\pi f_0 t} \tag{9}$$

$$= \int w_r(t-2|\mathbf{r}_{s,\boldsymbol{x}}|/c)\,w_a(s)\,\mathrm{e}^{\mathrm{i}2\pi\left(-2f_0|\mathbf{r}_{s,\boldsymbol{x}}|/c+\frac{K}{2}(t-2|\mathbf{r}_{s,\boldsymbol{x}}|/c)^2\right)}\,T(\boldsymbol{x})\,d\boldsymbol{x}. \tag{10}$$

3. MEASUREMENT MODEL FOR CSA

In CSA, the data processing starts in the range-time and azimuth-frequency domain (the range-Doppler domain). The first step of CSA is to approximate the kernel of the integral operator (10) in the range Doppler domain as follows:

$$d_0(s,t) \approx \int w_r\left(t-\frac{2\,|\mathbf{r}_{s_{\boldsymbol{x}},\boldsymbol{x}}|}{c_0\,D(f_s)}\right)\,W_a(f_s)\,\mathrm{e}^{\mathrm{i}\pi K_m\left[t-\frac{2\,|\mathbf{r}_{s_{\boldsymbol{x}},\boldsymbol{x}}|}{c_0\,D(f_s)}\right]^2}\,\mathrm{e}^{-\mathrm{i}\frac{4\pi\,|\mathbf{r}_{s_{\boldsymbol{x}},\boldsymbol{x}}|\,D(f_s)\,f_0}{c_0}}\,\mathrm{e}^{\mathrm{i}2\pi f_s(s-s_{\boldsymbol{x}})}\,df_s\,T(\boldsymbol{x})\,d\boldsymbol{x} \tag{11}$$

where W_a is the Fourier transform of w_a, $D(f_s) = \left(1-c_0^2\,f_s^2/[4|\mathbf{v}|^2 f_0^2]\right)^{-1/2}$ and K_m is given by $K/(1-KZ)$ with $Z(f_s,|\mathbf{r}_{s_{\boldsymbol{x}},\boldsymbol{x}}|) = c_0^2|\mathbf{r}_{s_{\boldsymbol{x}},\boldsymbol{x}}|f_s^2/[2|\mathbf{v}|^2 f_0^3 D^3(f_s)]$.[12]

(11) is obtained in 3 steps: i) performing the Fourier transform with respect to t leads to the kernel represented in range-temporal frequency, f_t and slow-time, s; ii) taking the Fourier transform with respect to s leads to the kernel represented in 2-D frequency domain, (f_t, f_s), where f_s denotes the azimuth-Doppler frequency; iii) performing the inverse Fourier transform with respect to f_t. Note that the method of stationary phase theorem is applied in every step.

Next, using the following identity for the unity:

$$1 = \int s_{sc}(\tau, f_s)\, \mathrm{e}^{i2\pi f_t(t-\tau)}\, s^*_{sc}(t, f_s) df_t d\tau \tag{12}$$

where $s_{sc}(\tau, f_s)$ is the *scaling function* given by[12]

$$s_{sc}(\tau, f_s) = \exp\left(\mathrm{i}\,\pi\, K_m \left[\frac{D(f_{s_{ref}})}{D(f_s)} - 1\right]\left[\tau - \frac{2\, r_{ref}}{c_0\, D(f_s)}\right]^2\right), \tag{13}$$

and s^*_{sc} is the complex conjugate of s_{sc}, we obtain

$$\begin{aligned} d_0(s,t) \approx \int w_r\left(\tau - \frac{2\,|\mathbf{r}_{s_{\boldsymbol{x}},\boldsymbol{x}}|}{c_0\, D(f_s)}\right) \mathrm{e}^{\mathrm{i}\pi K_m \frac{D(f_{s_{ref}})}{D(f_s)}\left[\tau - \left(\frac{2\,|\mathbf{r}_{s_{\boldsymbol{x}},\boldsymbol{x}}|}{c_0\, D(f_{s_{ref}})} + \left(\frac{1}{D(f_s)} - \frac{1}{D(f_{s_{ref}})}\right)\frac{2\, r_{ref}}{c_0}\right)\right]^2} \\ \times\ \mathrm{e}^{\mathrm{i}\frac{4\pi K_m}{c_0^2}\left[1 - \frac{D(f_s)}{D(f_{s_{ref}})}\right]\left[\frac{|\mathbf{r}_{s_{\boldsymbol{x}},\boldsymbol{x}}|}{D(f_s)} - \frac{r_{ref}}{D(f_s)}\right]^2} \mathrm{e}^{-\mathrm{i}2\pi f_t \tau} d\tau \\ \times\ W_a(f_s)\, \mathrm{e}^{-\mathrm{i}\frac{4\pi\,|\mathbf{r}_{s_{\boldsymbol{x}},\boldsymbol{x}}|\, D(f_s)\, f_0}{c_0}} [s_{sc}(t, f_s)]^{-1}\, \mathrm{e}^{\mathrm{i}2\pi f_s(s - s_{\boldsymbol{x}})}\, \mathrm{e}^{\mathrm{i}2\pi f_t t} df_t df_s\, T(\boldsymbol{x})\, d\boldsymbol{x} \end{aligned} \tag{14}$$

where r_{ref} and $f_{s_{ref}}$ are the reference range and reference azimuth frequency, respectively. Commonly, the target at the midrange of the scene is chosen to be the reference target in CSA, whose RCM is used as the reference for the scaling function to remove the residual range cell migration (RCM) of all the other targets. Therefore, r_{ref} is chosen to be the range of closest approach to the reference target and $f_{s_{ref}}$ is chosen to be the azimuth Doppler frequency at the time when the antenna beam center crosses the reference target. Note that as indicated by the phase center of the first exponential term in (14), by introducing the scaling function given by (13), the range variation of targets at different range cells are now the same with those of the targets at the reference range,r_{ref}.

Performing stationary phase approximation[10, 13, 14] with respect to τ integration, we approximate $d_0(s,t)$ in (14) by

$$d_0(s,t) \approx \int W_r(f_t)\, W_a(f_s)\, \mathrm{e}^{\mathrm{i}[\Phi_{CS}(|\mathbf{r}_{s_{\boldsymbol{x}},\boldsymbol{x}}|, f_s, f_t, t, \boldsymbol{x}) + 2\pi f_t t + 2\pi f_s(s - s_{\boldsymbol{x}})]} df_t df_s\, T(\boldsymbol{x})\, d\boldsymbol{x} \tag{15}$$

where W_r is the Fourier transform of w_r and

$$\begin{aligned} \Phi_{CS}(|\mathbf{r}_{s_{\boldsymbol{x}},\boldsymbol{x}}|, f_s, f_t, t, \boldsymbol{x}) = \Bigg(-\frac{\pi\, D(f_s)}{K_m\, D(f_{s_{ref}})}\, f_t^2 - \frac{4\,\pi\,|\mathbf{r}_{s_{\boldsymbol{x}},\boldsymbol{x}}|}{c_0\, D(f_{s_{ref}})}\, f_t - \frac{4\pi}{c_0}\left[\frac{1}{D(f_s)} - \frac{1}{D(f_{s_{ref}})}\right] r_{ref}\, f_t \\ - \frac{4\pi\,|\mathbf{r}_{s_{\boldsymbol{x}},\boldsymbol{x}}|\, f_0\, D(f_s)}{c_0} + \frac{4\pi\, K_m}{c_0^2}\left[1 - \frac{D(f_s)}{D(f_{s_{ref}})}\right]\left[\frac{|\mathbf{r}_{s_{\boldsymbol{x}},\boldsymbol{x}}|}{D(f_s)} - \frac{r_{ref}}{D(f_s)}\right]^2\Bigg) \\ - \pi\, K_m \left[\frac{D(f_{s_{ref}})}{D(f_s)} - 1\right]\left[t - \frac{2\, r_{ref}}{c_0\, D(f_s)}\right]^2. \end{aligned} \tag{16}$$

Let $\phi(f_t, f_s, s, t, \boldsymbol{x})$ and $A_{CS}(f_t, f_s)$ denote the phase terms and amplitude terms of (15), respectively, i.e.,

$$\phi(f_t, f_s, s, t, \boldsymbol{x}) = \Phi_{CS}(|\mathbf{r}_{s_{\boldsymbol{x}},\boldsymbol{x}}|, f_s, f_t, t, \boldsymbol{x}) + 2\pi f_t t + 2\pi f_s(s - s_{\boldsymbol{x}}), \tag{17}$$

$$A_{CS}(f_t, f_s) = W_r(f_t)\, W_a(f_s). \tag{18}$$

4. IMAGE FORMATION

In CSA, the data is modeled by (15) and an image I_{CS} of T is reconstructed by the following filtered back-projection operator $\mathcal{K}$:

$$I_{CS}(\boldsymbol{z}) := \mathcal{K}[d_0](\boldsymbol{z}) := \int \mathrm{e}^{-\mathrm{i}\phi(f_t,f_s,s,t,\boldsymbol{z})} Q_{CS}(f_t,f_s,t,s,\boldsymbol{z}) d_0(s,t) df_t df_s ds dt \tag{19}$$

where $\boldsymbol{z} = (z_1, z_2)$, $\mathbf{z} = (\boldsymbol{z}, 0)$, and Q_{CS} is the filter given by

$$Q_{CS}(f_t,f_s,t,s,\boldsymbol{z}) = W_r^*(f_t)\,. \tag{20}$$

We define the operator $\mathcal{L}_{CS} = \mathcal{K}\mathcal{F}$, which contains the information about how the image I_{CS} is related to the actual target scene T. We refer to the kernel $L_{CS}(\boldsymbol{z},\boldsymbol{x})$ of $\mathcal{L}_{CS}$ as the *point spread function*(PSF) of the CSA:

$$I_{CS}(\boldsymbol{z}) = \mathcal{K}\mathcal{F}[T](\boldsymbol{z}) = \mathcal{L}_{CS}[T](\boldsymbol{z}) = \int L_{CS}(\boldsymbol{z},\boldsymbol{x}) T(\boldsymbol{x}) d\boldsymbol{x}\,. \tag{21}$$

We will show that $\mathcal{L}_{CS}$ is a pseudo-differential operator.[9–11] Thus, I_{CS} has the edges of the scene at the right location and direction, but not at the right strength.

Substituting (15) in (19), the PSF of $\mathcal{L}_{CS}$ is given by

$$L_{CS}(\boldsymbol{z},\boldsymbol{x}) = \int \mathrm{e}^{-\mathrm{i}\phi(f_t',f_s',s,t,\boldsymbol{x})} \mathrm{e}^{-\mathrm{i}\phi(f_t,f_s,s,t,\boldsymbol{z})} Q_{CS}(f_t,f_s,t,s,\boldsymbol{z}) A_{CS}(f_t',f_s')\, df_t\, df_s\, df_t'\, df_s'\, d\,s\, d\,t. \tag{22}$$

Substituting (17) and (20) in (22) and performing the integrals with respect to s and f_s', respectively, we have

$$\begin{aligned} L_{CS}(\boldsymbol{z},\boldsymbol{x}) = \int & W_r^*(f_t) A_{CS}(f_t',f_s') \\ & \times \mathrm{e}^{-\mathrm{i}[\Phi_{CS}(|\mathbf{r}_{s_{\boldsymbol{z}},\boldsymbol{z}}|,f_s,f_t,t,\boldsymbol{z}) - \Phi_{CS}(|\mathbf{r}_{s_{\boldsymbol{x}},\boldsymbol{x}}|,f_s,f_t',t,\boldsymbol{x})]}\, \mathrm{e}^{\mathrm{i}2\pi f_s(s_{\boldsymbol{z}}-s_{\boldsymbol{x}})}\, \mathrm{e}^{\mathrm{i}2\pi t(f_t'-f_t)}\, df_t\, df_s\, df_t'\, dt. \end{aligned} \tag{23}$$

In (23), we make the change of variable $f_t' = u f_t$. Then, t and u integrals of (23) become

$$|f_t| \int A_{CS}(u f_t, f_s)\, \mathrm{e}^{\mathrm{i}\Phi_{CS}^{f_t',t}(|\mathbf{r}_{s_{\boldsymbol{x}},\boldsymbol{x}}|,f_s,u f_t,t,\boldsymbol{x})}\, \mathrm{e}^{\mathrm{i}2\pi t(u-1)f_t}\, dt du, \tag{24}$$

where $\Phi_{CS}^{f_t',t}$ denotes the part of $\Phi_{CS}(|\mathbf{r}_{s_{\boldsymbol{x}},\boldsymbol{x}}|, f_s, f_t', t, \boldsymbol{x})$ that involves f_t' and t.

We substitute (16) in (24), apply method of stationary phase with respect to u and t, and substitute the result back into (23) to obtain

$$L_{CS}(\boldsymbol{z},\boldsymbol{x}) \approx \int W_r^*(f_t)\, A_{CS}(f_t,f_s)\, \mathrm{e}^{\mathrm{i}[\Phi_{CS}(|\mathbf{r}_{s_{\boldsymbol{x}},\boldsymbol{x}}|,f_s,f_t,t_0,\boldsymbol{x}) - \Phi_{CS}(|\mathbf{r}_{s_{\boldsymbol{z}},\boldsymbol{z}}|,f_s,f_t,t_0,\boldsymbol{z})]}\, \mathrm{e}^{\mathrm{i}2\pi\, f_s(s_{\boldsymbol{z}}-s_{\boldsymbol{x}})} df_t\, df_s\,, \tag{25}$$

where t_0 is given by

$$t_0 = -\frac{D(f_s)}{K_m\, D(f_{s_{ref}})}\, f_t - \frac{2\,|\mathbf{r}_{s_{\boldsymbol{x}},\boldsymbol{x}}|}{c_0\, D(f_{s_{ref}})} - \frac{2}{c_0}\left[\frac{1}{D(f_s)} - \frac{1}{D(f_{s_{ref}})}\right] r_{ref}\,. \tag{26}$$

We linearize $\Phi_{CS}(|\mathbf{r}_{s_{\boldsymbol{x}},\boldsymbol{x}}|, f_s, f_t, t_0, \boldsymbol{x})$ and $s_{\boldsymbol{x}}$ around $\boldsymbol{x} = \boldsymbol{z}$:

$$\begin{aligned} \Phi_{CS}(|\mathbf{r}_{s_{\boldsymbol{x}},\boldsymbol{x}}|, f_s, f_t, t_0, \boldsymbol{x}) &\approx \Phi_{CS}(|\mathbf{r}_{s_{\boldsymbol{z}},\boldsymbol{z}}|, f_s, f_t, t_0, \boldsymbol{z}) + \nabla_{\boldsymbol{z}}\Phi_{CS}(|\mathbf{r}_{s_{\boldsymbol{z}},\boldsymbol{z}}|, f_s, f_t, t_0, \boldsymbol{z})\cdot(\boldsymbol{x}-\boldsymbol{z}), \\ s_{\boldsymbol{x}} &\approx s_{\boldsymbol{z}} + \nabla_{\boldsymbol{z}} s_{\boldsymbol{z}}\cdot(\boldsymbol{x}-\boldsymbol{z}). \end{aligned} \tag{27}$$

Thus, (25) can be approximated by

$$L_{CS}(\boldsymbol{z},\boldsymbol{x}) \approx \int \mathrm{e}^{\mathrm{i}\nabla_{\boldsymbol{z}}[\Phi_{CS}(|\mathbf{r}_{s_{\boldsymbol{z}},\boldsymbol{z}}|,f_s,f_t,t_0,\boldsymbol{z}) + 2\pi f_s s_{\boldsymbol{z}}]\cdot(\boldsymbol{x}-\boldsymbol{z})}\, W_r^*(f_t)\, A_{CS}(f_t,f_s)\, df_t\, df_s\,. \tag{28}$$

For fixed $\boldsymbol{x}$ and $\boldsymbol{z}$, we make the change of variable

$$(f_t, f_s) \to \boldsymbol{\xi} = \nabla_{\boldsymbol{z}}[\Phi_{CS}(|\mathbf{r}_{s_{\boldsymbol{z}},\boldsymbol{z}}|, f_s, f_t, t_0, \boldsymbol{z}) + 2\pi f_s s_{\boldsymbol{z}}] \tag{29}$$

in (28), and obtain

$$L_{CS}(\boldsymbol{z}, \boldsymbol{x}) \approx \int_{\Omega_{\boldsymbol{\xi}}} \mathrm{e}^{\mathrm{i}(\boldsymbol{x}-\boldsymbol{z})\cdot\boldsymbol{\xi}}\, W_r^*(f_t(\boldsymbol{\xi}))A_{CS}(f_t(\boldsymbol{\xi}), f_s(\boldsymbol{\xi}))\left|\frac{\partial(f_t, f_s)}{\partial\boldsymbol{\xi}}\right| d\boldsymbol{\xi} \tag{30}$$

where $\Omega_{\boldsymbol{\xi}} = \{\boldsymbol{\xi} : \boldsymbol{\xi} = \nabla_{\boldsymbol{z}}[\Phi_{CS}(|\mathbf{r}_{s_{\boldsymbol{z}},\boldsymbol{z}}|, f_s, f_t, t_0, \boldsymbol{z}) + 2\pi f_s s_{\boldsymbol{z}}],\ \forall f_s, f_t\}$ is referred to as the data collection manifold,[3] which characterizes the frequency content of the reconstructed image. $|\partial(f_t, f_s)/\partial\boldsymbol{\xi}|$ is the determinant of the Jacobian that comes from the change of variables (29).

(30) shows that the operator $\mathcal{L}_{\mathcal{CS}}$ as a pseudo-differential operator,[9–11] which implies that the edges are reconstructed at the right location and direction. Substituting (30) into (21), we obtain

$$I_{CS}(\boldsymbol{z}) \approx \int_{\Omega_{\boldsymbol{\xi}}} \mathrm{e}^{\mathrm{i}(\boldsymbol{x}-\boldsymbol{z})\cdot\boldsymbol{\xi}}\, W_r^*(f_t(\boldsymbol{\xi}))A_{CS}(f_t(\boldsymbol{\xi}), f_s(\boldsymbol{\xi}))\left|\frac{\partial(f_t, f_s)}{\partial\boldsymbol{\xi}}\right| T(\boldsymbol{x}) d\boldsymbol{x} d\boldsymbol{\xi}\,. \tag{31}$$

Thus I_{CS} puts the edges of T at the right location and direction, but not at the right strength.

In order to reconstruct the edges with the right strength, we change the filter in (20) to:

$$Q_{CS}(f_t, f_s, t, s, \boldsymbol{z}) = \frac{A_{CS}^*(f_t, f_s)}{|A_{CS}(f_t, f_s)|^2}\left|\frac{\partial\boldsymbol{\xi}}{\partial(f_t, f_s)}\right|. \tag{32}$$

With this choice of filter, the PSF is now approximately a Dirac delta function:

$$L_{CS}(\boldsymbol{z}, \boldsymbol{x}) \approx \int_{\Omega\boldsymbol{\xi}} \mathrm{e}^{\mathrm{i}(\boldsymbol{x}-\boldsymbol{z})\cdot\boldsymbol{\xi}}\, d\boldsymbol{\xi}\,. \tag{33}$$

Thus, the edges are reconstructed not only at the right location and direction, but also at the right strength.

5. CONCLUSION

In this paper, we presented a new treatment of the CSA from the perspective of FIO theory. We showed that the imaging operator in CSA can be viewed as a backprojection operator and that the associated point spread function is the kernel of a pseudo-differential operator. Pseudo-differential operators have pseudo-local property which puts the edges of the scene at the right location and direction in the reconstructed image, but not at the right strength.

We determined a new filter to ensure that the reconstructed edges are not only at the right location and direction, but also at the right strength. As a result, the new chirp scaling based imaging method can be viewed as a generalized filtered-backprojection type inversion. Our approach has the potential to extend the chirp-scaling based imaging to non-ideal imaging imaging scenarios involving arbitrary flight trajectories and non-flat topography as well as to other SAR modalities such as bistatic and hitchhiker SAR.

REFERENCES

[1] Yarman, C. E., Yazıcı, B., and Cheney, M., "Bistatic synthetic aperture radar imaging for arbitrary flight trajectories," *IEEE Transactions on Image Processing* **17** (January 2008).

[2] Yarman, C. E. and Yazıcı, B., "Synthetic aperture hitchhiker imaging," *IEEE Transactions on Image Processing* **17**, 2156–2173 (November 2008).

[3] Yazici, B., Cheney, M., and Yarman, C. E., "Synthetic-aperture inversion in the presence of noise and clutter," *Inverse Problems* **22**, 1705–1729 (2006).

[4] Yarman, C., Yazici, B., and Cheney, M., "Bistatic synthetic aperture hitchhiker imaging with non-cooperative sources of opportunity," in [*Proceedings of SPIE Defense and Security Symposium*], 65806 (April 2007).

[5] Nolan, C. J. and Cheney, M., "Synthetic aperture inversion," *Inverse Problems* **18**, 221–236 (2002).
[6] Nolan, C. and Cheney, M., "Synthetic aperture inversion for arbitrary flight paths and non-flat topography," *IEEE Transactions on Image Processing* **12**, 1035–1043 (2003).
[7] Herman, G., Tuy, H. K., Langenberg, K., and Sabatier, P., [*Basic Methods of Tomography and Inverse Problems*], Adam Hilger, Philadelphia, PA (1988).
[8] Langenberg, K., Brandfass, M., Mayer, K., Kreutter, T., Brüll, A., Felinger, P., and Huo, D., "Principles of microwave imaging and inverse scattering," *EARSeL Adv. Remote Sens.* **2**, 163–186 (1993).
[9] Duistermaat, J. J., [*Fourier Integral Operators*], Birkhauser, Boston (1996).
[10] Grigis, A. and Sjöstrand, J., [*Microlocal Analysis for Differential Operators: An Introduction*], London Mathematical Society Lecture Note Series, Vol. 196, Cambridge University Press, Cambridge (1994).
[11] Treves, F., [*Introduction to Pseudodifferential and Fourier Integral Operators, volumes I and II*], Plenum Press, New York (1980).
[12] Cumming, I. G. and Wong, F. H., [*Digital Processing Of Synthetic Aperture Radar Data: Algorithms And Implementation*], Artech House Remote Sensing Library (2005).
[13] Bleistein, N. and Handelsman, R., [*Asymptotic Expansions of Integrals*], Dover, New York (1986).
[14] Guillemin, V. and Sternberg, S., [*Geometric Asymptotics*], American Math. Society, Providence (1979).